BUILD SIMUL (2015) 8: 551 – 565
DOI 10.1007/s12273-014-0227-6

The ventilation needed to control thermal plume and particle dispersion from manikins in a unidirectional ventilated protective isolation room

Caiqing Yang[1,2], Xudong Yang[1] (✉), Bin Zhao[1]

1. Department of Building Science, School of Architecture, Tsinghua University, Beijing 100084, China
2. School of Aerospace Engineering, Tsinghua University, Beijing 100084, China

Abstract

Infection is a major cause of death for the immunocompromised patients whose immune mechanisms are deficient. The most effective way of protecting these patients is the total environment protection such as protective isolation room (PIR). Unidirectional airflow ventilation is usually used in PIR. The supply air velocity in PIR can affect not only the cleanliness level of the room and total environment protection effects to the patients, but also the energy consumption and initial equipment investment of the room. Computational fluid dynamics (CFD) program is used to simulate the airflow field and the concentration distribution of the particles from human body and breathing. Three scenarios when the manikin is standing, sitting and lying are investigated in this study. The intensities of supply airflow with different velocities and the upward airflow induced by thermal plume with different postures are compared. The qualitative and quantitative analysis of the simulation results show that the required supply air velocity to control the thermal plume and particle dispersion from human body and breathing is at least 0.25 m/s when the manikin is standing or sitting, and 0.2 m/s when the manikin is lying.

Keywords

unidirectional airflow ventilation,
computational fluid dynamics (CFD),
air distribution,
protective isolation

Article History

Received: 30 December 2014
Revised: 7 April 2015
Accepted: 14 April 2015

1 Introduction

Severe and often prolonged neutropenia is the inevitable consequence of chemotherapy for leukaemia and lymphoma, and conditioning regimens for bone marrow transplantation. Life-threatening infection is an inevitable consequence for many of these patients. Single room isolation with positive airflow produced by unidirectional airflow units should be used for those patients who are most at risk of aspergillosis (Fenelon 1995). The existing research indicated an appropriate air filtration system combining with unidirectional airflow ventilation could prevent bacterial infections and increase survival rate effectively (Storb et al. 1983; Barnes and Rogers 1989; Passweg et al. 1998; Schlesinger et al. 2009). Unidirectional airflow moves "in a single direction and in parallel layers at constant velocity from the beginning to the end of a straight-line vector" (Gregory et al. 2007). Hence, the unidirectional airflow ventilation system could control airborne particulate contamination by direct entrainment and removal.

Protective isolation room (PIR) is used to protect the patients whose immune mechanisms are deficient or compromised. Unidirectional ventilation is widely used in these environments. The clean air treated by the high efficiency particulate air (HEPA) filters is usually supplied to the protective isolation room from the ceiling and returned from the return openings located at the bottom of the walls. To create unidirectional airflow in the room, the supply opening is usually mounted on up to proportion of 90% or more of the ceiling area. When the supply air velocity is too small, the ventilation may fail to create a protective environment for the patients in the room. Instead, if the supply air velocity is too high, the treated and transported airflow rate is huge and lead to very high energy consumption. Therefore, the proper supply air velocity is an important parameter in unidirectional ventilated PIR.

Many researchers have investigated the ventilation and dispersion of airborne particles or droplets in airborne infection isolation room (AIIR) where patients with known or suspected infectious disease that spread via airborne particles or droplets are housed. Both experimental (Tung et al. 2009a; Johnson et al. 2009; Bolashikov et al. 2012; Tang

E-mail: xyang@tsinghua.edu.cn

et al. 2013; Leung et al. 2013) and simulation approaches (Tung et al. 2009b; Qian and Li 2010; Chen et al. 2011; Memarzadeh and Xu 2012; Ghia et al. 2012) were used in the research. Although PIR and AIIR are both patient wards, they have apparent differences. AIIR uses negative-pressure ventilation and the purpose of ventilation is to avoid spread of pathogen-carrying particles from the patients. Instead, PIR uses positive-pressure ventilation and the purpose of ventilation is to protect patients from being infected by others. Also researchers have studied the ventilation, airborne or droplets transmission characteristics in operating theatres (OT) where surgical-site infections are a major problem (Friberg et al. 2003; Chow and Yang 2005; Chow et al. 2006; Liu et al. 2009; Zoon et al. 2011; Balocco et al. 2012; Chow and Wang 2012). The ventilation in both PIR and OT intends to create a unidirectional airflow environment to protect the patients. But they also have great differences. The patients in OT cannot move during the operation, it is thus easier to create a protective environment in specified small zone in the room. The patients in PIR may change their postures (sitting, lying or standing) and walk around, creating a small area unidirectional ventilation protection is not enough and a total environment protection is needed. The using time of OT is usually very short, each operation only lasts for several hours. But in PIR, a patient maybe stay for many days or even months. The main disturbances to the airflow in the OT are lights, equipment used in the operating, doctors, nurses and patient. In PIR, the main disturbance to the airflow is the patient in the ward. Due to the differences among AIIR, OT and PIR discussed above, the study results of AIIR and OT may not be applicable in PIR. Very few researchers have studied and investigated the ventilation and airborne particle dispersion in PIR. Hence, this study is important and essential for the researchers and engineers who worked on PIR related area.

The occupant in the PIR is a major heat and pollution source, the convective flow generated by the human body has a significant impact on the room air distribution and contaminant transmission (Salmanzadeh et al. 2012). Several researches in the past have investigated the convective boundary layer around a human body in indoor environment. Lewis et al. (1969) investigated the microenvironment around the human and found that starting from the feet, there is a layer of air which passes up adjacent to the surface of the body, its thickness progressively increasing as it rises and accelerates. Clark and Toy (1975) investigated the natural convection around the human head and found the convective flow patterns around the human head vary markedly with body posture. Homma and Yakiyama (1988) revealed that the mean velocity in the convective boundary layer around a human body is up to 0.25 m/s. Voelker et al. (2014) measured the air temperature and flow velocity in the human body's microclimate and found the higher the temperature difference between the surface temperature of the manikin and the air temperature, the faster the airflow in the microclimate. Licina et al. (2014) examined the influence on temperature difference between the human body surface and room air temperature, and found that the increase of the ambient temperature from 20 to 26℃ widen the convective boundary layer flow in front of the sitting manikin but does not influence the shape of the standing manikin. To create a total protective environment, the vertical unidirectional ventilation must control the thermal plume created by the human body effectively. Larger supply air velocity can have a better control of the thermal plume, but requires higher initial investment and operating energy consumption. To determine the proper supply air velocity is thus essential for the engineering design of the system. The key research point of this study is the interaction between the thermal plume from human body and airflow filed created by the ventilation system in PIR. Some existing studies have investigated the interaction between the thermal plume and indoor ventilation. Johnson et al. (1996) studied airflow interaction between the human free convection flow and ventilation in a low-speed uniform environment. Yang et al. (2009a) studied the interaction of the personalized airflow supplied from ceiling mounted nozzle with the thermal plume generated by a seated thermal manikin. Licina et al. (2015) investigated the interaction between the human convective boundary layer and uniform airflow with different velocity and from different directions. Some studies numerically investigated the particle transport under the combined action of thermal plume and ventilation (Li et al. 2013; Ge et al. 2013). In this study, the airflow and particle transmission characteristics in the PIR with different supply air velocities were simulated and analyzed. Three scenarios when the manikin is standing, sitting and lying were considered to examine the strength of the upward airflow induced by thermal plume when people were in different postures. The optimal supply air velocities for the three scenarios to control thermal plume and particle dispersion in PIR are recommended.

2 Research methods

2.1 Mathematic model

The airflow is assumed to be at steady state, three-dimensional, incompressible and turbulent. Based on these assumptions, the time-averaged Navier-Stokes and continuity equations are given by

$$\frac{\partial\left(U_j U_i\right)}{\partial x_j} = -\frac{1}{\rho_a}\frac{\partial P}{\partial x_i} + \frac{\partial}{\partial x_j}\left(\nu\frac{\partial U_i}{\partial x_j} - \overline{u_i' u_j'}\right) \quad (1)$$

$$\frac{\partial U_i}{\partial x_i} = 0 \tag{2}$$

where x_i are Cartesian coordinates, U_i are the components of the mean velocity, P is the mean pressure, ρ_a is the density of air, ν is the kinematic viscosity and $\overline{u_i' u_j'}$ is the Reynolds-stress tensor that is unknown and needs modeling in order to obtain a closed set of equations.

In this study, CFD software Fluent 6.3 (Fluent 2005) was used to simulate the airflow and particle concentration in the unidirectional ventilated protective isolation room. Chen (1995) reviewed and compared eight modified k–ε models and found that the RNG k–ε model developed by Yakhot et al. (1992) performed the best among all the eddy-viscosity models tested for mixed convection flows. Rouaud and Havet (2002) used both standard and RNG k–ε turbulence models to simulate the airflow in a food-processing clean room. Both models predicted the main features of the airflow and the numerical results agreed with experimental data, while the RNG k–ε model predicted more swirls and more complex trajectories. Therefore, we adopted the RNG k–ε turbulence model in this study to simulate the airflow. The RNG k–ε turbulence model, accruing from the renormalization group mathematical theory, is supposed to correct the k–ε model's deficiency in determining the turbulence kinetic energy, by adding an extra source term to the turbulence kinetic energy dissipation (ε) transport equation and having slightly different constants compared to the k–ε model (Yakhot and Orszag 1986; Smith and Reynolds 1992; Yakhot et al. 1992; Yakhot and Smith 1992).

We measured the particle concentration of different size in downward unidirectional ventilated PIR and found the concentrations for larger particles (particles larger than 1 μm) were all quite low in the room. The concentrations of those particles in the locations 0.6 m outside the particle emission source were almost 0 (Yang 2012). That was because the larger particles were easier to be controlled by the downward ventilation due to the effect of gravity. However, smaller particles were easily influenced by the upward airflow induced by thermal plume from human body and therefore, more difficult to be controlled by the downward ventilation. This study mainly focused the transmission characteristics of small particles. The particle size in this study was about 0.5 μm, which was of great concern in clean rooms. The maximal permitted particle concentration for particles with 0.5 μm in ISO cleanliness Class 5 clean room was 3520 pcs/m^3 (pcs: particles) (Yang et al. 2009b). Zhao and Wu (2005) indicated that the nominal time of a ventilated room and the particle relaxation time may be a good indicator to decide if the particle can be treated as passive contaminant. If the value of indicator was small, the particle could be treated as passive contaminant. We calculated the indicators of the particles in PIR and found that when the particle size was no larger than 10 μm, the indicators of the particles were all lower than the upper limit (2.8E–02 s^2) suggested by Zhao and Wu (2005). Hence, the particles with size no larger than 10 μm could be treated as passive contaminant in PIR. Chen et al. (2006) simulated particle distribution and deposition in indoor environments with a new drift-flux model and also indicated that the particles smaller than 2 μm shared the common dispersion and transport properties of air. Halthway et al. (2011) indicated that passive scalar was appropriate for small particles. Therefore, the particles of 0.5 μm in this study were treated as gaseous contaminant. The control equation used to calculate the concentration of particles was as follows:

$$\frac{\partial}{\partial t}(\rho C_p) + \nabla \cdot (\rho C_p \overrightarrow{u_i}) = \nabla \cdot \left(\frac{\mu_{eff}}{\sigma_C} \nabla C_p\right) + S_p \tag{3}$$

where ρ is the density of air (kg/m^3); C_p is particle concentration (pcs/m^3); $\overrightarrow{u_i}$ is the velocity of the air (m/s); σ_C is the turbulent diffusivity of C_p, the value was set as 1.0 in this study. S_p is the emission rate per unit volume of the particle source (pcs/(m^3·s)). μ_{eff} is the sum of molecular (μ) and turbulent dynamic viscosity (μ_t).

2.2 Model validation

We performed full scale field measurements of airflow and particle concentration distribution in an ISO-Class-5 clean room in a hospital. Figure 1 presents the configuration of the clean room and its adjacent bathroom and the locations of the test points. The size of the clean ward was 3.3 m (length-X) × 2.5 m (height-Y) × 3.1 m (width-Z), within which the bathroom accounts for a space sizing 1.5 m (length-X) × 2.5 m (height-Y) × 1.4 m (width-Z). Clean air was supplied into the clean ward through ceiling-mounted high efficiency particulate air (HEPA) filters with the opening size of 3.1 m (X) × 1.5 m (Z) plus 1.6 m (X) × 1.3 m (Z) in clean ward. The supply airflow rate was 6950 m^3/h, which was corresponding to 341 air changes per hour (ACH) in the clean ward. The air was exhausted from the air return openings located at the bottom of the two sidewalls of the clean ward, with each return air opening sizes being 0.3 m (Y) × 0.75 m (Z). In the meanwhile, part of the airflow supplied to the clean ward entered the bathroom via door gaps due to higher air pressure of clean ward compared to the bathroom. The size of the door gap was 0.02 m (Y) × 0.8 m (Z). We measured the pressure difference between the two sides of the door and calculated the infiltration airflow rate from the clean ward to bathroom through the door gap, which is 100 m^3/h. The clean supply air opening was fully

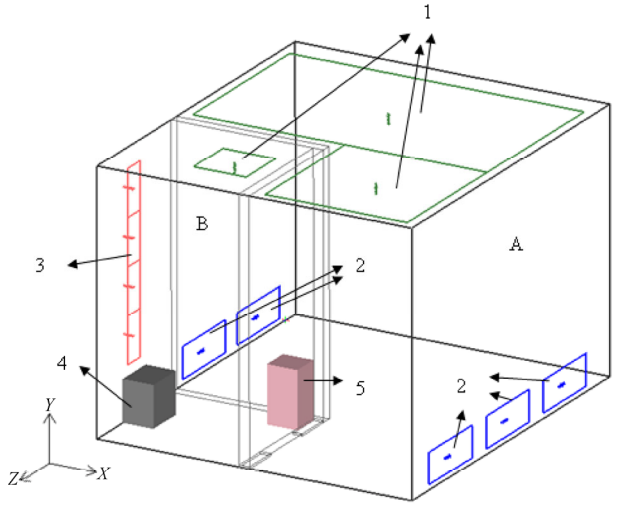

(a) Configuration of the tested clean ward

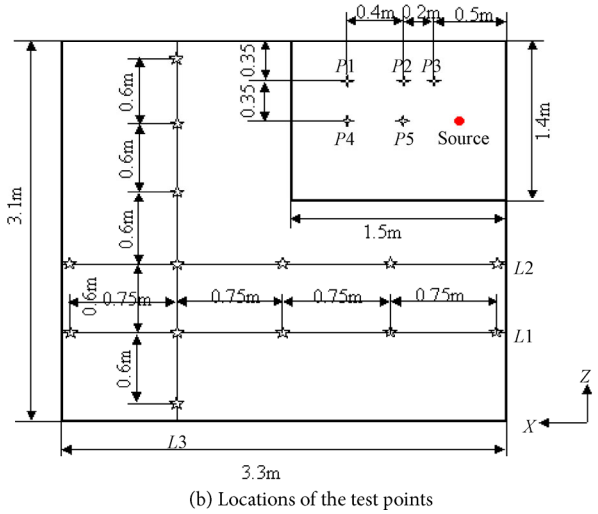

(b) Locations of the test points

Fig. 1 Configuration of the tested clean ward (A: patient care room, B: bathroom, 1: air supply openings, 2: air return openings, 3: air exhaust, 4: toilet tank, 5: particle generator.) and the locations of the test points

covered by HEPA filters with the size of 0.5 m (X) × 0.5 m (Z) in the bathroom. The air exhaust vent run vertically along the near wall of the bathroom, with opening size being 1.8 m (Y) × 0.2 m (Z). The supply and exhaust airflow rates in the bathroom were 325 m^3/h and 425 m^3/h, respectively. Hot sphere anemometers (RHAT-301) were used to measure the air velocity in the ventilated space. The anemometers can measure velocities ranging from 0.05 to 5.00 m/s with a precision of 0.1 m/s, or a precision ±3% of reading higher than 0.1 m/s. A condensation mono-disperse aerosol generator (TSI 3475, TSI Inc.) was used to generate the fine diethylhexyl sebacate (DEHS) particles to simulate the point particle source in the toilet. We used FLUKE 983 optical particle counters to measure the particle concentration in the room. Detailed information about the field test in the clean ward and the instruments used in the measurements was introduced in (Yang et al. 2009b).

The measured and simulated air velocities at measurement locations in the room are plotted in Fig. 2. Considering the experiment was conducted in real protective isolation room instead of lab. The comparisons show that the simulated velocities agree well with the experimental data. The relative error is less than 10% for 80% of the measurement points. Figure 3 presents the comparison of simulated and measured particle concentrations. In this study, the concentration of $P4$ at the height of 0.28 m in the bathroom was used as the reference concentration to calculate the dimensionless concentration, which is the highest concentration among all the tested points and different from the study of our previous sutdy (Yang et al. 2009b). Experiment in real protective isolation room is harder than in lab. To have a good match of the tested data with simulated data is very challenging. The comparing of the tested and simulated particle concentrations in Fig. 3 is good enough for the data collected in real protective isolation room. The particle simulation model used in this study is reliable.

2.3 Investigated scenarios

The validated CFD model was further applied to investigate the particle dispersion from the manikin in the PIR. The size of the room investigated in this study was 3 m × 2.5 m × 3 m (length-X, height-Y, and width-Z). The supply opening was located in the ceiling with the size of 3 m × 3 m (length-X and width-Z). The air was exhausted from the outlets located at the bottom of two sidewalls of the room, with each opening size being 0.3 m × 3 m (height-Y, and width-Z). One breathing thermal manikin was located at the center of the room. The doctor or nurse is usually in a standing position when walking into the clean ward, but the patient may be in a standing, sitting or lying position. Here, we simulated the scenarios when the manikin is standing, sitting and lying and examined the proper supply air velocity to control the thermal plume and contaminant from manikin in these three positions. Thus, three scenarios when the thermal manikin was standing (Scenario 1), sitting (Scenario 2) and lying (Scenario 3) were simulated and analyzed separately. The schematic diagram of the three scenarios is shown in Fig. 4. The height of the standing and sitting manikin was 1.7 m and 1.24 m, respectively. The geometry of the lying manikin was of the same shape and size with the standing manikin. The mesh of the central plane used in the three scenarios is shown in Fig. 5. The number of cells used in Scenarios 1, 2 and 3 is 3.5 million, 2.5 million and 2.5 million, respectively.

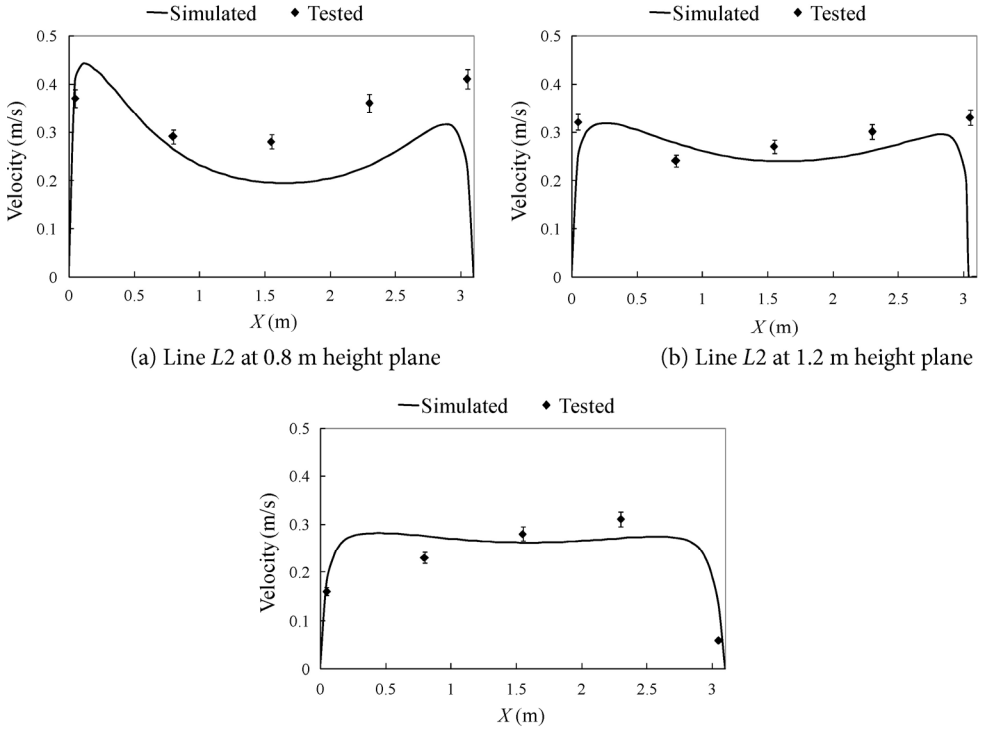

(a) Line *L*2 at 0.8 m height plane

(b) Line *L*2 at 1.2 m height plane

(c) Line *L*2 at 1.6m height plane

Fig. 2 Simulated and measured air velocities of *L*2 at three heights in the clean ward

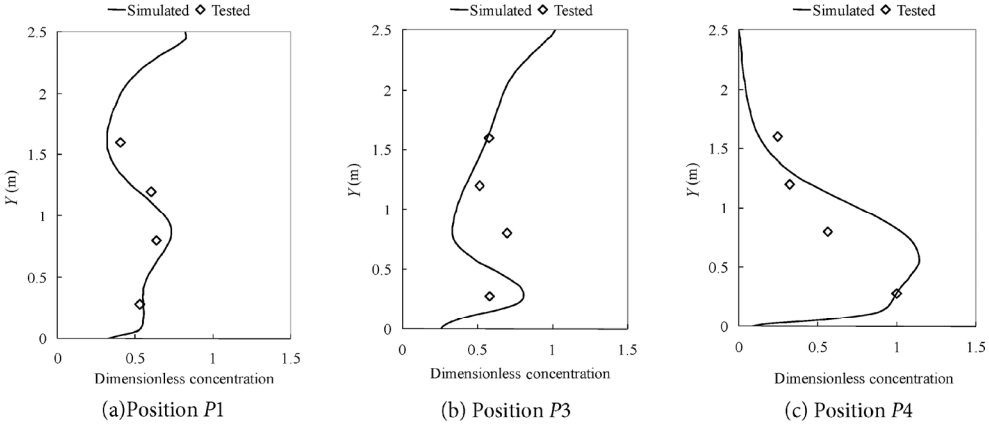

(a)Position *P*1

(b) Position *P*3

(c) Position *P*4

Fig. 3 Simulated and tested dimensionless particle concentration profiles at three measurement locations in the bathroom

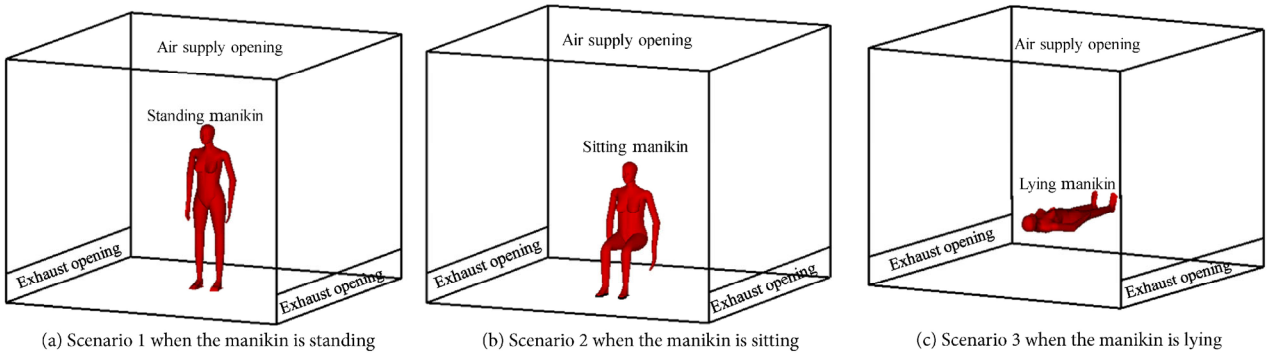

(a) Scenario 1 when the manikin is standing

(b) Scenario 2 when the manikin is sitting

(c) Scenario 3 when the manikin is lying

Fig. 4 Schematic diagram of simulated scenarios

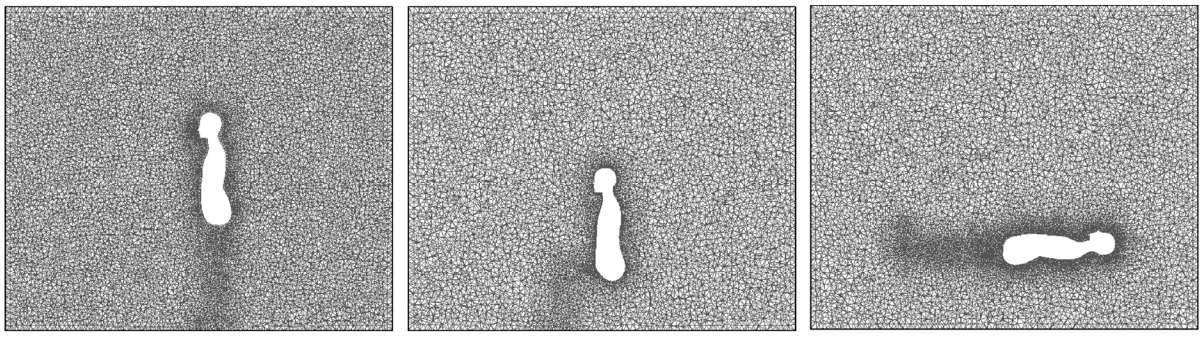

(a) Scenario 1 (3.5 million cells) (b) Scenario 2 (2.5 million cells) (c) Scenario 3 (2.5 million cells)

Fig. 5 Mesh of the central surface used in the three scenarios

Neumann boundary condition which equals the mass flow rate between the inlet and outlet was applied at the outlet. The inlet was set to have a given velocity, and the supply air temperature was fixed at 24℃ which was recommended by GB 50457-2008 (2009). Most of the walls in the PIR were interior walls and had little heat transfer through the walls. The heat flux of walls and floor was set to 0.

To predict the effect of occupants on indoor airflow, one would need to consider more sophisticated boundary conditions (Deevy et al. 2008). Dygert et al. (2009) indicated that the strength of the thermal plume is relatively insensitive to the temperature distribution on the human body surface, as long as the area-weighted average temperature on the human body surface is the same. Existing human simulation usually assigned a uniform temperature to the body surface in numerical simulation, and the body surface temperature ranged from 28℃ to 33.7℃ (Murakami et al. 1999; Jakie et al. 2010; Zhang et al. 2011; Salmanzadeh et al. 2012; Li et al. 2013). Jackie et al. (2010) calculated the intake fraction (iF) in the indoor environment when the body surface was fixed at 32℃ and 28℃ and found that a 4℃ change in body surface temperature influenced the intake fraction by less than 10%. The upward airflow induced by thermal plume from the human body is the major concern in the protective isolation room. Higher surface temperature creates higher thermal plume and need larger ventilation rate. If the assigned body surface temperature in the simulation is too low, the calculated ventilation rate needed to control the thermal plume may not be sufficient in actual conditions. Therefore, we assigned a uniform surface body temperature of 33℃ when the manikin was standing, sitting or lying. The total heat flux generated by the manikin's body was about 75 W.

Both the patient and doctor/nurse had no strenuous activities in the ward. They sat or lay on the bed or stood on the floor with slight movement for most of the time. The bacteria, fungi, dust and other various contaminants in the air may deposit onto the clothes. The contaminants on clothes dressed by the patient and doctor/nurse will re-suspend to the air. The fiber of the clothes will also release to the indoor air. The particles produced by the clothes are assumed to be emitted from human body in this study. We used the emitting rate of particles of 0.5 μm or larger from a seated person dressed in ordinary work clothes to simulate the particle dispersion in the clean ward. The particle generation rate from a human body was 3.02×10^5 particles per minute (Yang et al. 2009b). The particle emitting rate from breathing was also set to 3.02×10^5 particles per minute in order to compare the particle dispersion characteristics from human body and breathing. From the research of McFadden et al. (1985), the average temperature in the upper trachea was in a range of 32 ± 0.05℃, thus the temperature of breathing air from thermal manikin's nose was set to 32℃ in this study. The exhaled air speed has a wide span due to the sinusoidal-like respiration rhythm. The peak expiratory flow rate for normal breathing is about 0.4 L/s (Gupta et al. 2010). We used the peak expiratory flow rate to simulate the breathing, in order to investigate the influence of breathing to the airflow in the most unfavorable conditions.

3 Results and discussion

3.1 Scenario 1 (the manikin is standing)

The airflow fields for Scenario 1 (the manikin is standing) with different supply air velocities are shown in Fig. 6. The size of interference region of the thermal plume from the thermal manikin is decreasing with the increase of supply air velocity. When the supply air velocity is 0.05 m/s, the upward airflow induced by thermal plume from manikin can disrupt most of the downward airflow in the room and create a huge interference region. But, when the supply air velocity reaches 0.25 m/s, only the airflow near the thermal manikin can be disrupted by the thermal plume, the interference region of the thermal plume is very small. By comparing the airflow field at different supply air velocities,

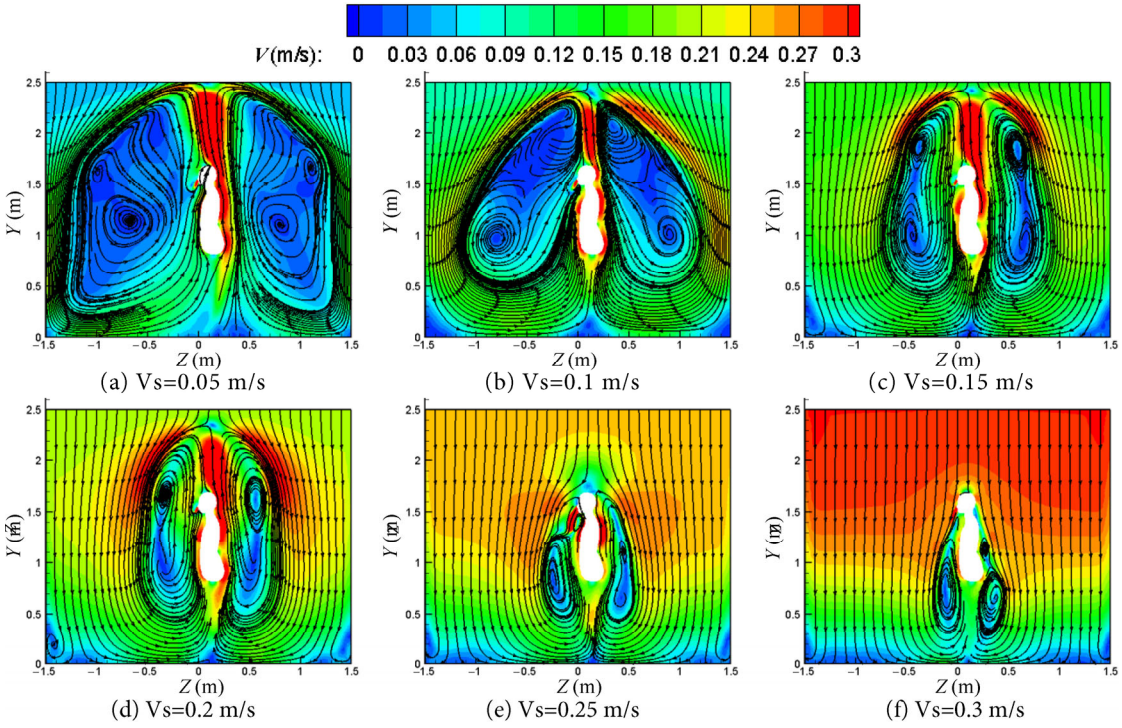

Fig. 6 Airflow fields for Scenario 1 with different supply air velocities (Vs is supply air velocity)

we found that the supply air velocity should be no less than 0.25 m/s in order to control the thermal plume from a standing thermal manikin. The intensity of the upward airflow induced by thermal plume from a standing manikin is larger than the supply airflow when the supply air velocity is smaller than or equal to 0.2 m/s.

The particle concentration distribution from human body and breathing for Scenario 1 with different supply air velocities is shown in Fig. 7. The particle dispersion range is decreasing with the increase of supply air velocity. The particles from breathing mainly transport in the zone in front of the manikin, while particles from human body can transport to all directions in the room. The dispersion range of the particles from human body is obviously larger than the dispersion range from breathing. When supply velocity is 0.05 m/s，the particles from breathing can spread to most of the space in front of the manikin and particles from the human body can spread to almost the entire room. The particle concentrations in the room remain to be high until the supply air velocity reaches 0.25 m/s, when particles from both breathing and human body are well controlled by the ventilation air. Thus, to control the particle dispersion in the PIR with a standing manikin, the supply air velocity should be no less than 0.25 m/s.

3.2 Scenario 2 (the manikin is sitting)

The airflow fields for Scenario 2 (the manikin is sitting) with different supply air velocities are shown in Fig. 8. Same with Scenario 1, the size of interference region of the thermal plume from manikin is also decreasing with the increase of the supply air velocity. The air near the human body flows upward and creates a vortex region near the human body when the supply air velocity is smaller than or equal to 0.2 m/s. When the supply air velocity is 0.05 m/s, the thermal plume from manikin could disrupt most of the downward airflow in the room and create a huge interference region. When the supply air velocity is 0.2 m/s, the upward airflow induced by thermal plume from manikin could still spread to 2 m height in the room. As the supply air velocity reaches 0.25 m/s, only the airflow near the manikin can be disrupted by the thermal plume from human body, and the interference region of the thermal plume is very small. The comparison of airflow fields shows that when the supply air velocity is higher than 0.25 m/s, the thermal plume from a sitting manikin can be well controlled by the ventilation in the PIR.

Licina et al. (2015) investigated the interaction between the human convective boundary layer and downward flow with different velocities. The breathing of manikin was ignored in their study. To compare with their results, we simulated the airflow fields of a sitting manikin in the PIR without breathing. The comparison of the airflow in breathing zone between our results and theirs is shown in Fig. 9. Comparing Figs. 9 (a) and (b), we can see that, the airflow in breathing zone when the supply air velocity is

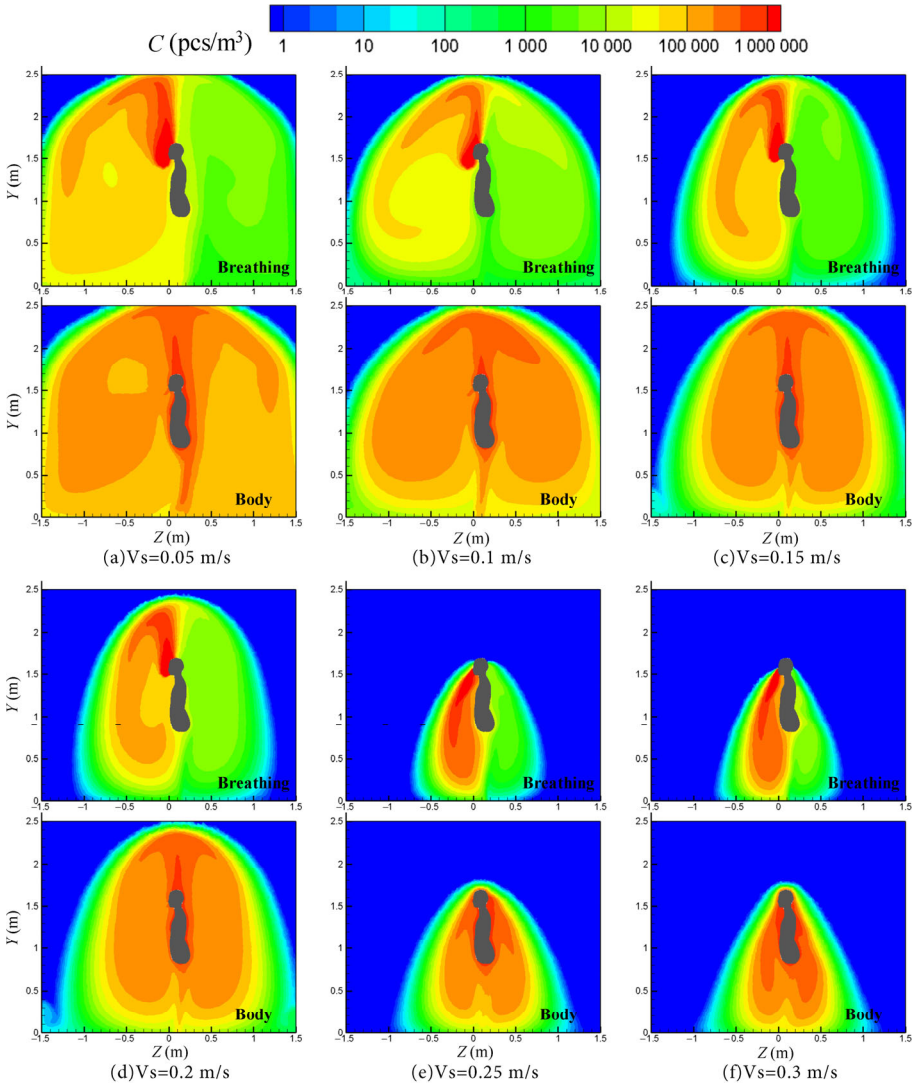

Fig. 7 Particle concentration distribution for Scenario 1 with different supply air velocities (Vs is supply air velocity)

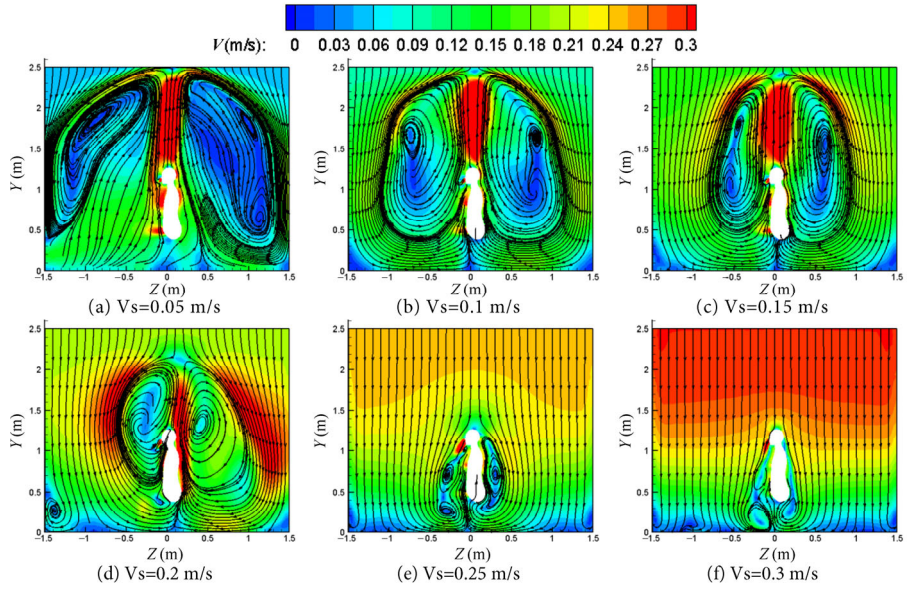

Fig. 8 Airflow fields for Scenario 2 with different supply air velocities (Vs is supply air velocity)

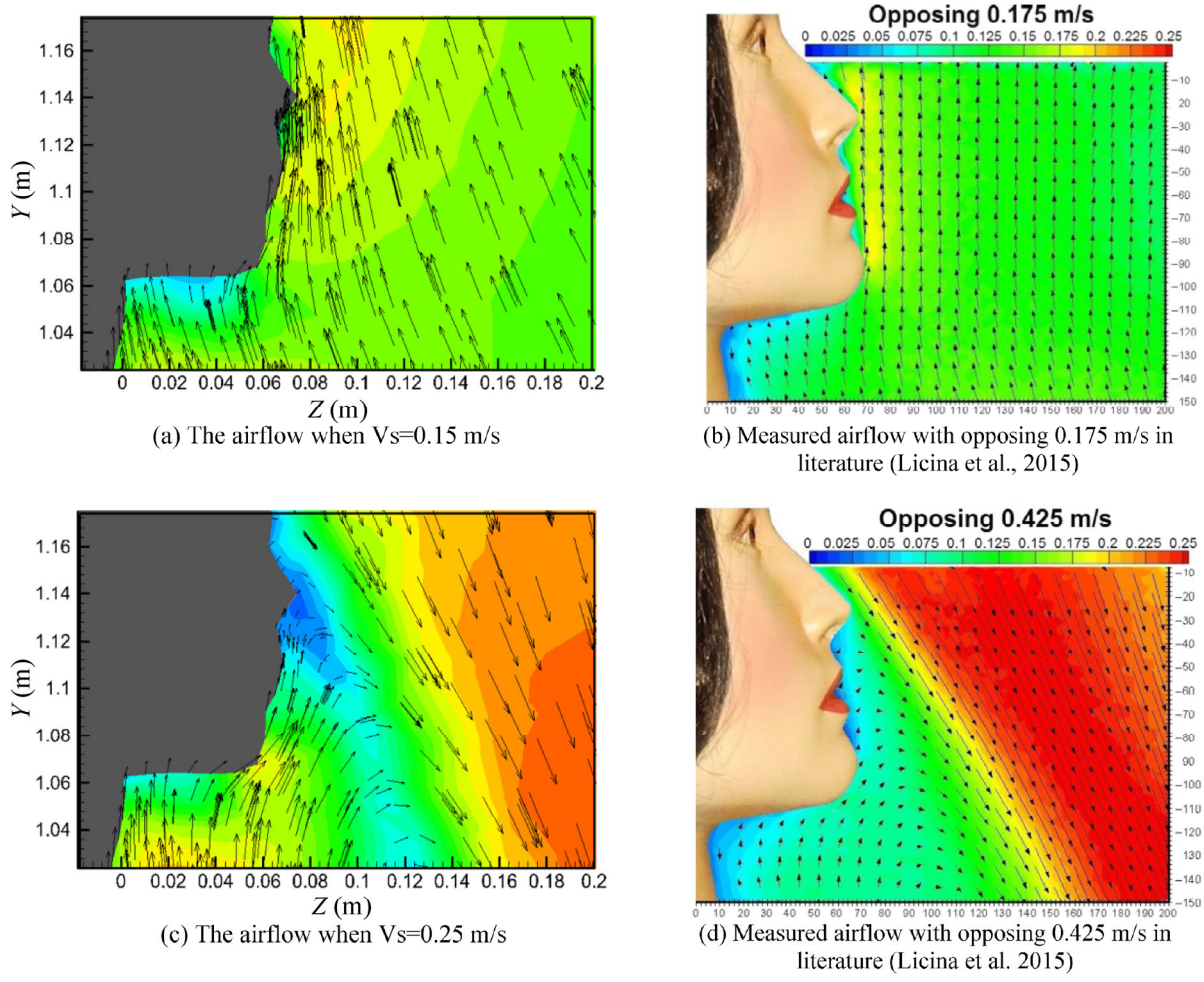

(a) The airflow when Vs=0.15 m/s

(b) Measured airflow with opposing 0.175 m/s in literature (Licina et al., 2015)

(c) The airflow when Vs=0.25 m/s

(d) Measured airflow with opposing 0.425 m/s in literature (Licina et al. 2015)

Fig. 9 Comparison of the simulated airflow with downward unidirectional ventilation in this study and measured airflow with downward ventilation in the literature in the breathing zone when the manikin is sitting

0.15 m/s is similar with the airflow with opposing 0.175 m/s in their study. The airflow directions near the manikin are all upward and the upward airflow speeds induced by the thermal plume are all around 0.15 m/s. By comparing Figs. 9(c) and (d), we can see that, the airflow in breathing zone when the supply air velocity is 0.25 m/s is similar with the airflow with opposing 0.425 m/s in their study. The downward ventilations are all break away the human thermal plume and create a predominantly downward airflow in front of the face. The down ward airflow speed in our study near the manikin is slightly lower than that in their study. The upward thermal plume can be well controlled by the downward ventilation when the supply air velocity is 0.25 m/s. The airflow near the manikin in the breathing zone with downward ventilation when the manikin is sitting matches well with the research of Licina et al. (2015), which further verifies the reliability of the simulation results.

The particle concentration distribution from human body and breathing for Scenario 2 with different supply air velocity is shown in Fig. 10. The particle dispersion range is also decreasing with the increase of supply air velocity. The particles from breathing and from human body are carried by the airflow near the human body to the upper space and spread in the vortex region near the human body. The dispersion region of the particles is very large when the supply air velocity is smaller than or equal to 0.2 m/s. As the supply air velocity reaches 0.25 m/s, the particles from breathing and human body are carried by the downward airflow and discharged from the exhausts located at the bottom of sidewalls. The particle concentration is very low and the particles only spread in small zone around the human body.

3.3 Scenario 3 (the manikin is lying)

Figure 11 presents the airflow fields when the manikin is lying. The size of the interference region of the thermal plume from manikin is also decreasing with the increase

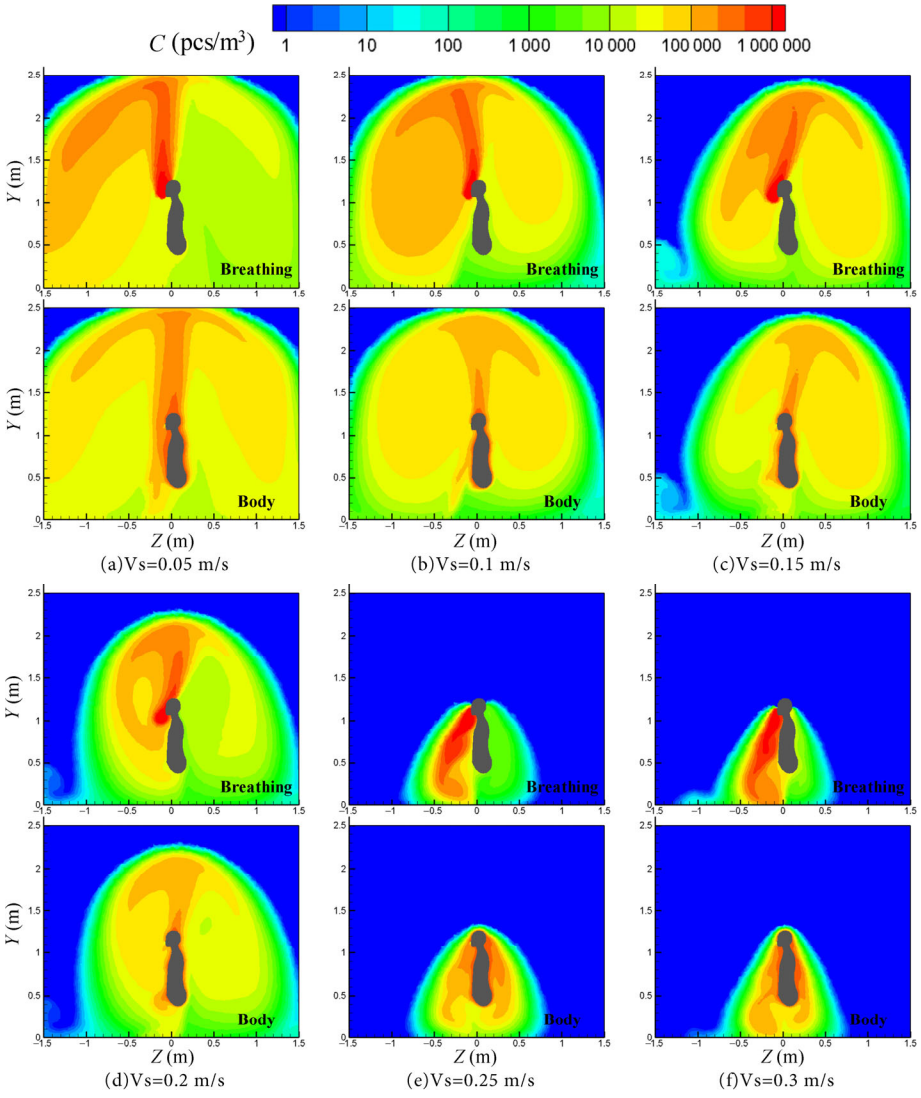

Fig. 10 Particle concentration distribution for Scenario 2 with different supply air velocities (Vs is supply air velocity)

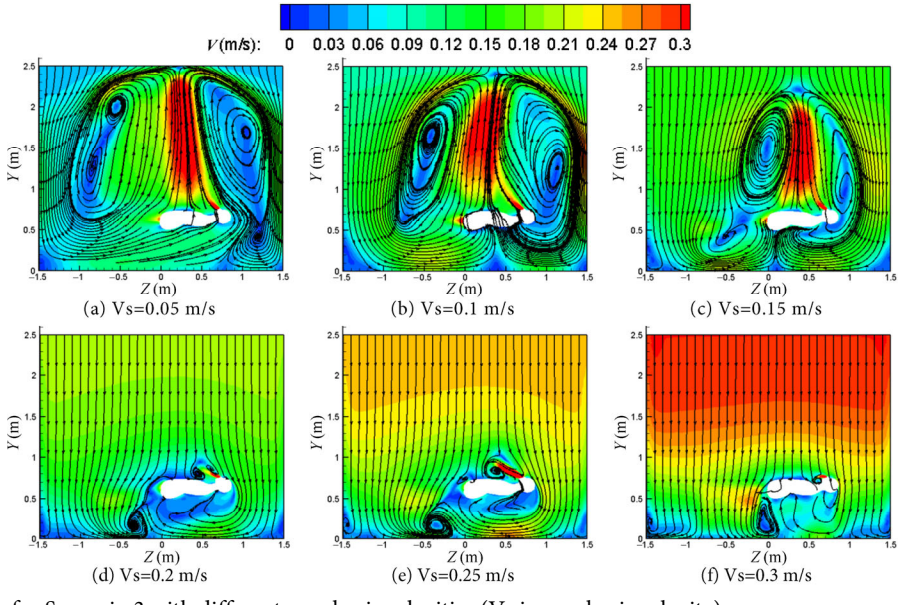

Fig. 11 Airflow fields for Scenario 3 with different supply air velocities (Vs is supply air velocity)

of the supply air velocity. When the supply air velocity is smaller than or equal to 0.15 m/s, the airflow of the whole room is controlled by the upward airflow induced by thermal plume from the human body. The intensity of upward airflow induced by thermal plume is larger than the intensity of supply airflow at this time. The upward airflow induced by thermal plume from the manikin can reach the ceiling when the supply velocity is 0.05 m/s. When the supply air velocity reaches 0.2 m/s, the intensity of the upward airflow induced by thermal plume is smaller than the intensity of supply airflow, and the upward thermal plume is well controlled by the downward supply airflow.

The particle concentration fields for Scenario 3 when the manikin is lying are shown in Fig. 12. When the supply air velocity is smaller than or equal to 0.15 m/s, the particles emitted from human body or breathing can spread to a large region. As the supply air velocity reaches 0.2 m/s, the particles from human body and breathing are well controlled by the supply airflow and only spread in a quite small region around the human body.

3.4 Quantitative analysis

There are mainly two airflows in the PIR, the supply airflow and the upward airflow induced by the human thermal plume. The upward airflow induced by thermal plume will break the unidirectional airflow from supply and lead to pollutant transmission in the room. Only when the intensity of the

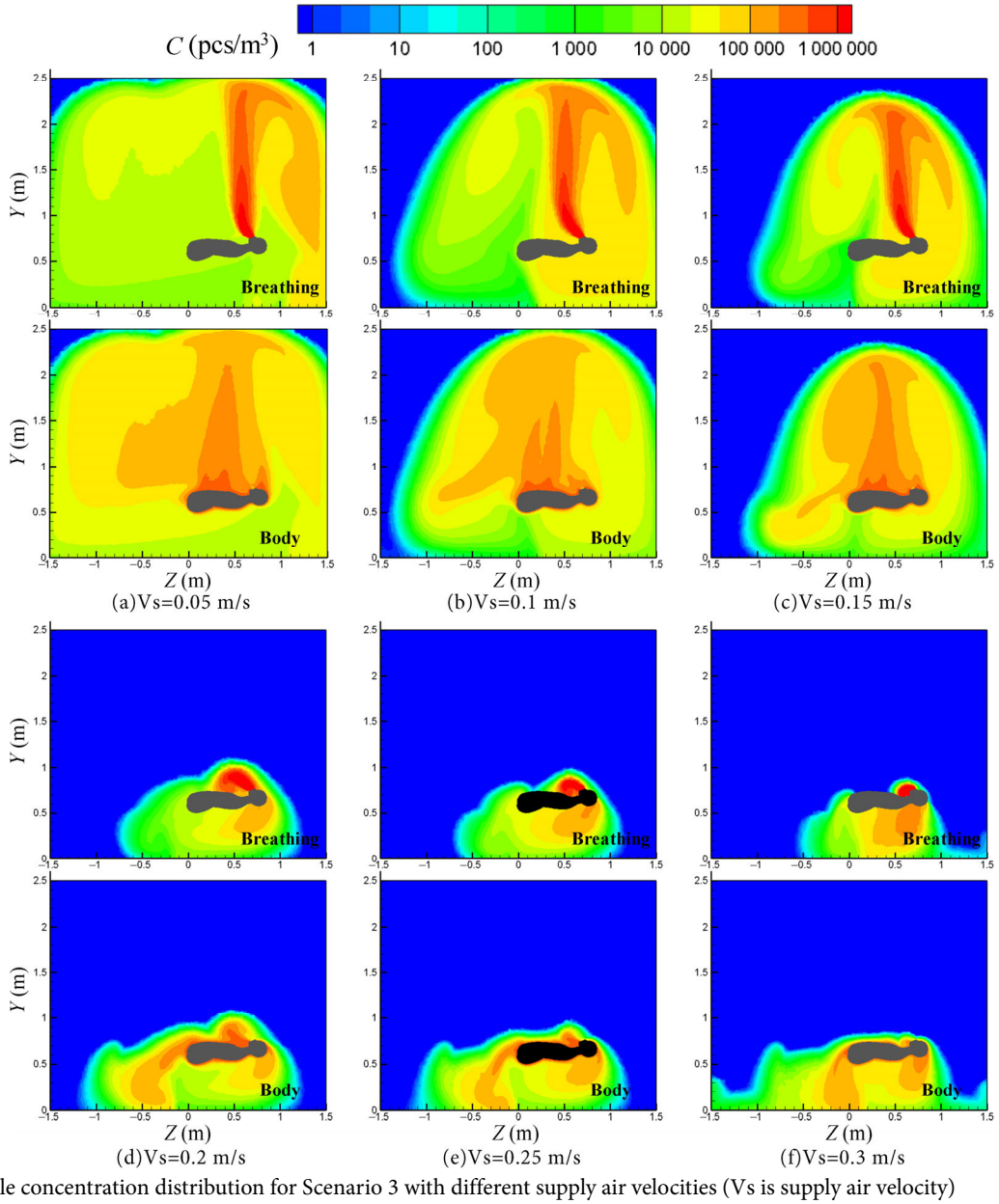

Fig. 12 Particle concentration distribution for Scenario 3 with different supply air velocities (Vs is supply air velocity)

supply air is large enough to control the thermal plume, the airflow in the room can maintain unidirectional state.

We calculated the Reynolds number of supply air with different supply air velocities. The Reynolds number is defined as (Incropera and DeWitt 1990):

$$Re = \frac{\rho VD}{\mu} \tag{4}$$

where V is the mean velocity of supply air (m/s); D is the hydraulic diameter of the air supply opening (m), set to 3.0 m in this study; μ is the dynamic viscosity of the air, (kg/(m·s)); ρ is the density of the air (kg/m^3).

The Re range of the upward airflow induced by the thermal plume from a manikin can be estimated from the qualitative analysis in Section 3.1–3.3. The comparison of the Reynolds number of supplied airflow and upward airflow induced by thermal plume is shown in Fig. 13. The comparison shows that the intensity of supply airflow increases with the increase of the supply air velocity. When the supply air velocity is no less than 0.2 m/s, the intensity of supply airflow is larger than the intensity of the upward airflow induced by thermal plume from lying manikin. When the supply air velocity is no less than 0.25 m/s, the intensity of supply airflow is larger than that of the upward airflow induced by thermal plume from standing or sitting manikin. The airflow induced by the thermal plume of a standing manikin is stronger than that induced by the thermal plume of a lying manikin. Clark and Toy (1975) also found the convective flow near the manikin varied markedly with body postures. From their study, the velocity of the flow over the head of a standing subject can exceed 0.3 m/s, by contrast, the velocity of the flow over the horizontal head reaches only 0.05 m/s. When the supply air velocity reaches to 0.25 m/s, the thermal plume of the standing manikin and sitting manikin can be well controlled in our study. When the supply air velocity reaches to 0.2 m/s, the thermal plume from lying manikin can be well controlled.

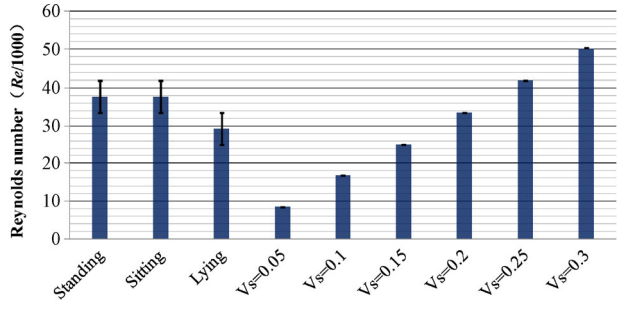

Fig. 13 Comparison of Reynolds number of supply airflow (in m/s) and upward airflow induced by manikin thermal plume

For the three Scenarios, the air cleanness level in the PIR is also calculated at the breathing height. The breathing heights are defined as 1.7 m, 1.2 m, and 0.75 m when the manikin is standing, sitting, and lying, respectively. Borrowing the definition of airborne particulate cleanliness classes in ISO Standard 14644-1 (1999), the classification of air cleanliness in clean rooms and associated controlled environments is defined in terms of concentration of airborne particles within the space. The relationship among the maximal permitted particle concentration that is allowed, ISO cleanliness class, and the associated diameter of the particles of concern is

$$C_n = 10^N \times \left(0.1/d\right)^{2.08} \tag{5}$$

where C_n is the maximum-permitted number of particle counts per cubic meter equal to or larger than the specified particle size (d) (pcs/m^3); N is the ISO cleanliness class number, which must be a multiple of 0.1 and be 9 or less; d is the particle size in micrometers (μm). The maximal permitted particle concentration for particles with 0.5 μm in ISO cleanliness Class 5 clean room is 3520 pcs/m^3.

The particle concentrations at breathing heights are shown in Fig. 14. For Scenario 1 (when the manikin is standing) and Scenario 2 (when the manikin is sitting), the particle concentration from breathing and human body at breathing height is much lower than the maximum-permitted particle concentration for ISO-Class-5 when the supply air velocity reaches 0.25 m/s. Lowering the supply air velocity cannot guarantee the particle concentration for ISO-Class-5. For Scenario 3 (when the manikin is lying), ISO-Class-5 can be obtained when the supply air velocity reach to 0.2 m/s.

The recommended supply air velocity is 0.25 m/s for Scenarios 1 and 2, and 0.2 m/s for Scenario 3 from the analysis above. The temperature fields under the recommended supply air velocity of the three scenarios are shown in Fig. 15. From the figure, we can see that, the indoor temperature is almost equal to the supply air temperature. Although the supply air velocity is low, the size of supply opening is big (supply opening is fully mounted on the ceiling), the ventilation rate is high. The air change per hour when the supply air velocity is 0.2 m/s and 0.25 m/s is 288 ACH and 360 ACH, respectively. The huge ventilation rate leads to small temperature difference between supply air and return air. The indoor air temperature is uniform and almost equal the supply air temperature.

Based on the discussions above, the required supply air velocity when the manikin is lying could be smaller than that when the manikin is standing or sitting. Since the

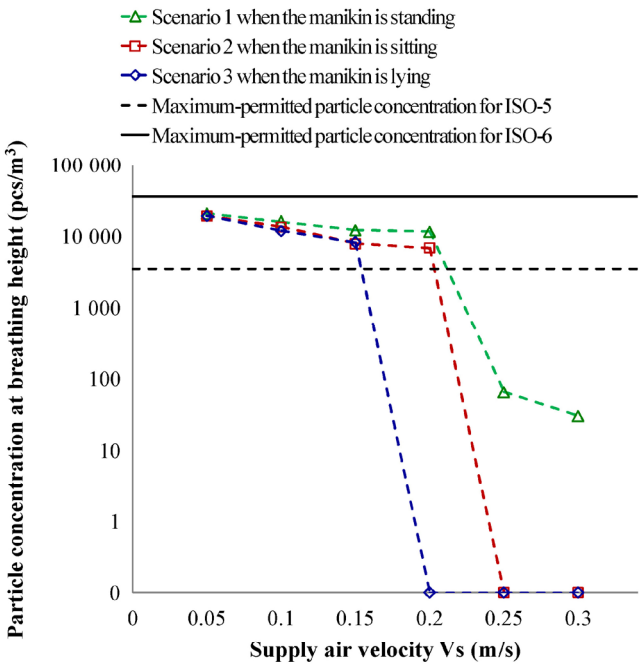

(a) Particles emitted from human breathing

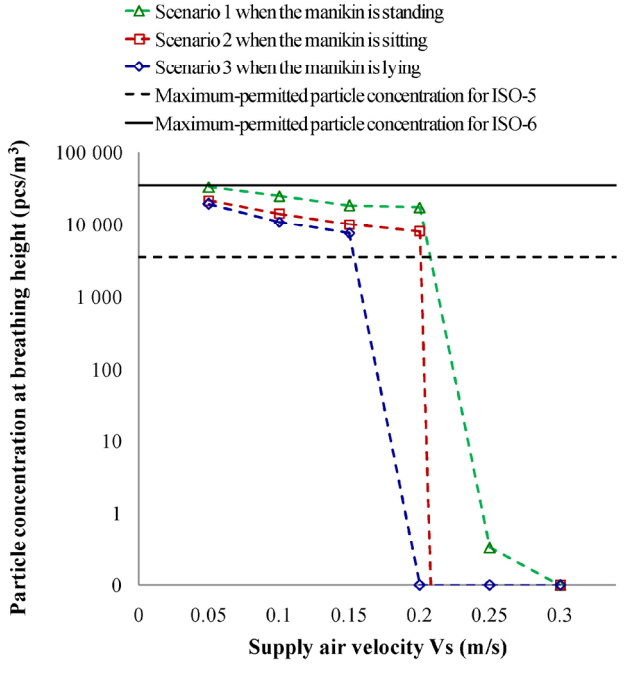

(b) Particles emitted from human body

Fig. 14 Particle concentration at breathing height

patients in the ward may sit on bed or walk around (in standing posture) in the ward at daytime but lie in bed and sleep at night, the PIR could use different supply air velocities at day time and night. The supply air velocity could be set to 0.25 m/s during the day time and 0.2 m/s at night. This can reduce energy consumption on the premise of high cleanliness level of the PIR.

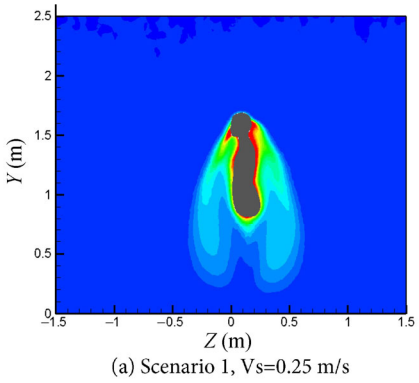

(a) Scenario 1, Vs=0.25 m/s

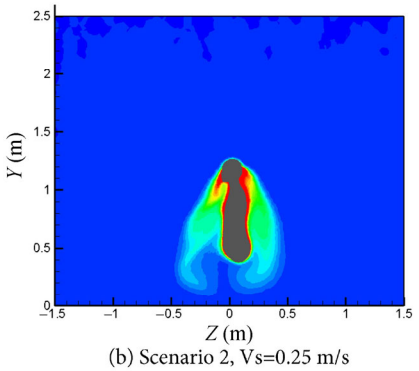

(b) Scenario 2, Vs=0.25 m/s

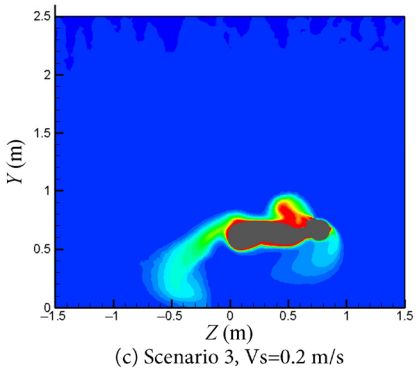

(c) Scenario 3, Vs=0.2 m/s

Fig. 15 Temperature fields under the recommended supply air velocity of the three scenarios

4 Conclusions

Computational fluid mechanics (CFD) program is used to simulate the airflow field and the dispersion of the particles from human body and breathing in PIR. Three scenarios when the manikin is standing, sitting and lying are investigated. The following conclusions can be reached:

(1) To control the thermal plume and particle dispersion in PIR and create a clean and safe environment for the patients, the supply air velocity should be around 0.25 m/s when the manikin is standing or sitting, and 0.2 m/s when the manikin is lying.

(2) In order to save operating energy, the PIR could use high supply velocity (0.25 m/s) during day time and switch to lower supply velocity (0.2 m/s) at night.

Acknowledgements

This project is supported by the National Natural Science Foundation of China (No. 51178237).The authors would like to thank Professor Yuguo Li and his research group for kindly providing their manikin models.

References

Balocco C, Petrone G, Cammarata G (2012). Assessing the effects of sliding doors on an operating theatre climate. *Building Simulation*, 5: 73–83.

Barnes RA, Rogers TR (1989). Control of an outbreak of nosocomial aspergillosis by laminar air-flow isolation. *Journal of Hospital Infection*, 14:89–94.

Bolashikov ZD, Melikov AK, Kierat W, Popiolek Z, Brand M (2012). Exposure of health care workers and occupants to coughed airborne pathogens in a double-bed hospital patient room with overhead mixing ventilation. *HVAC&R* Research, 18: 602–615.

Chen C, Zhao B, Yang X, Li Y (2011). Role of two-way airflow owing to temperature difference in severe acute respiratory syndrome transmission: Revisiting the largest nosocomial severe acute respiratory syndrome outbreak in Hong Kong. *Journal of the Royal Society Interface*, 8: 699–710.

Chen F, Yu S, Lai A (2006). Modeling particle distribution and deposition in indoor environments with a new drift-flux model. *Atmospheric Environment*, 40: 357–367.

Chen Q (1995). Comparison of different *k*–epsilon models for indoor air flow computations. *Numerical Heat Transfer Part B*: *Fundamentals*, 28: 353–369.

Chow TT, Wang J (2012). Dynamic simulation on impact of surgeon bending movement on bacteria-carrying particles distribution in operating theatre. *Building and Environment*, 57: 68–80.

Chow TT, Yang XY (2005). Ventilation performance in the operating theatre against airborne infection: Numerical study on an ultra-clean system. *Journal of Hospital Infection*, 59: 138–147.

Chow TT, Zhang L, Bai W (2006). The integrated effect of medical lamp position and diffuser discharge velocity on ultra-clean ventilation performance in an operating theatre. *Indoor and Built Environment*, 15: 315–331.

Clark RP, Toy N (1975). Natural convection around the human head. *Journal of Physiology*, 244: 283–293.

Deevy M, Sinai Y, Everitt P, Voigt L, Gobeau N (2008). Modelling the effect of an occupant on displacement ventilation with computational fluid dynamics. *Energy and Buildings*, 40: 255–264.

Dygert RK, Dang TQ, Russo JS, Khalifa HE (2009). Modelling of the human body to study the personal micro environment. *ASHRAE Transactions*, 115 (2): 407–420.

Fenelon LE (1995). Protective isolation: Who needs it? *Journal of Hospital Infection*, 30 (Supplement): 218–222.

FLUENT (2005). FLUENT Version 6.2. Lebanon, NH, USA: Fluent Inc.

Friberg S, Ardnor B, Lundholm R, Friberg B (2003). The addition of a mobile ultra-clean exponential laminar airflow screen to conventional operating room ventilation reduces bacterial contamination to operating box levels. *Journal of Hospital Infection*, 55: 92–97.

GB 50457-2008 (2009). Code for Design of Pharmaceutical Industry Clean Room. Beijing: China Planning Press. (in Chinese)

Ge Q, Li X, Inthavong K, Tu J (2013). Numerical study of the effects of human body heat on particle transport and inhalation in indoor environment. *Building and Environment*, 59: 1–9.

Ghia U, Konangi S, Kishore A, Gressel M, Mead K, Earnest G (2012). Assessment of health-care worker exposure to pandemic flu in hospital rooms. *ASHRAE Transactions*, 118(1): 442–449.

Gregory FP, Marghi RM, Willianm TW (2007). Potential for airborne contamination in turbulent-and unidirectional-airflow compounding aseptic isolators. *American Journal of Health-System Pharmacy*, 64: 622–631.

Gupta JK, Lin CH, Chen Q (2010). Characterizing exhaled airflow from breathing and talking. *Indoor Air*, 20: 31–39.

Halthway EA, Noakes CJ, Sleigh PA, Fletcher LA (2011). CFD simulation of airborne pathogen transport due to human activities. *Building and Environment*, 46: 2500–2511.

Homma H, Yakiyama M (1988). Examination of free convection around occupant's body caused by its metabolic heat. *ASHRAE Transactions*, 94(1): 104–124.

Incropera F, DeWitt D (1990). Fundamentals of Heat and Mass Transfer. New York: John Wiley and Sons.

International Organization for Standardization (ISO) (1999). ISO 14644-1, Cleanrooms and Associate Controlled Environments—Part 1—Classification of Air Cleanliness. Arlington Heights, IL, USA: The Institute of Environmental Sciences and Technology (IEST).

Jackie S, Russo H, Ezzat K (2010). CFD assessment of intake fraction in the indoor environment. *Building and Environment*, 45: 1968–1975.

Johnson AE, Fletcher B, Saunders CJ (1996). Air movement around a worker in a low-speed flow field. *Annals of Occupational Hygiene*, 40: 57–64.

Johnson DL, Lynch RA, Mead KR (2009). Containment effectiveness of expedient patient isolation units. *American Journal of Infection Control*, 37: 94–100.

Leung WT, Sze-To GN, Chao CYH, Yu SCT, Kwan JKC (2013). Study on the interzonal migration of airborne infectious particles in an isolation ward using benign bacteria. *Indoor Air*, 23: 148–161.

Lewis HE, Foster AR, Mullan BJ, Cox RN, Clark RP (1969). Aerodynamics of the human microenvironment. *Lancet,* 322: 1273–1277.

Li X, Inthavong K, Ge Q, Tu J (2013). Numerical investigation of particle transport and inhalation using standing thermal manikins. *Building and Environment*, 60: 116–125.

Licina D, Melikov A, Sekhar C, Tham KW (2015). Human convective boundary layer and its interaction with room ventilation flow. *Indoor Air*, 25: 21–35.

Licina D, Pantelic J, Melikov A, Sekhar C, Tham KW (2014). Experimental investigation of the human convective boundary layer in a quiescent indoor environment. *Building and Environment*, 75: 79–91.

Liu J, Wang H, Wen W (2009). Numerical simulation on a horizontal airflow for airborne particles control in hospital operating room. *Building and Environment*, 44: 2284–2289.

McFadden ER, Pichurko BM, Bowman HF, Ingenito E, Burns S, Dowling N, Solway J (1985). Thermal mapping of the airways in humans. *Journal of Applied Physiology*, 58: 564–570.

Memarzadeh F, Xu W (2012). Role of air changes per hour (ACH) in possible transmission of airborne infections. *Building Simulation*, 5: 15–28.

Murakami S, Zeng J, Hayashi T (1999). CFD analysis of wind environment around a human body. *Journal of Wind Engineering and Industrial Aerodynamics*, 83: 393–408.

Passweg JR, Rowlings PA, Atkinson KA, Barrett AJ, Gale RP, Gratwohl A, Jacobsen N, Klein JP, Ljungman P, Russell JA, Schaefer UW, Sobocinski KA, Vossen JM, Zhang MJ, Horowitz MM (1998). Influence of protective isolation on outcome of allogeneic bone marrow transplantation for leukemia. *Bone Marrow Transplantation*, 21: 1231–1238.

Qian H, Li Y (2010). Removal of exhaled particles by ventilation and deposition in a multibed airborne infection isolation room. *Indoor Air*, 20: 284–297.

Rouaud O, Havet M (2002). Computation of the airflow in a pilot scale clean room using k–ε turbulence models. *International Journal of Refrigeration*, 25: 351 – 361.

Salmanzadeh M, Zahedi G, Ahmadi G, Marr DR, Glauser M (2012). Computational modeling of effects of thermal plume adjacent to body on the indoor airflow and particle transport. *Journal of Aerosol Science*, 53: 29–39.

Schlesinger A, Paul M, Gafter-Gvili A, Rubinovitch B, Leibovici L (2009). Infection-control interventions for cancer patients after chemotherapy: A systematic review and meta-analysis. *The Lancet Infectious Diseases*, 9: 97–107.

Smith LM, Reynolds WC (1992). On the Yakhot-Orszag renormalization group method for deriving turbulence statistics and models. *Physics of Fluids A*: *Fluid Dynamics*, 4: 364–390.

Storb R, Prentice RL, Buckner CD, Clift RA, Appelbaum F, Deeg J, Doney K, Hansen JA, Mason M, Sanders JE, Singer J, Sullivan KM, Witherspoon, RP, Thomas ED (1983). Graft versus host disease and survival in patients with aplastic anaemia treated by marrow grafts from HLA-identical siblings-Beneficial effect of a protective environment. *New England Journal of Medicine*, 308: 302–307.

Tang JW, Nicolle A, Pantelic J, Klettner CA, Su R, Kalliomaki P, Saarinen P, Koskela H, Reijula K, Mustakallio P, Cheong DKW, Sekhar C, Tham KW (2013). Different types of door-opening motions as contributing factors to containment failures in hospital isolation rooms. *PLOS ONE*, 8(6): e66663. doi:10.1371/journal.pone.0066663.

Tung Y-C, Hu S-C, Tsai T-I, Chang I-L (2009a). An experimental study on ventilation efficiency of isolation room. *Building and Environment*, 44: 271–279.

Tung Y-C, Shih Y-C, Hu S-C (2009b). Numerical study on the dispersion of airborne contaminants from an isolation room in the case of door opening. *Applied Thermal Engineering*, 29: 1544–1551.

Voelker C, Maempel S, Kornadt O (2014). Measuring the human body's microclimate using a thermal manikin. *Indoor Air*, 24: 567–579.

Yakhot V, Orszag SA (1986). Renormalization group analysis of turbulence I. Base theory. *Journal of Scientific Computing*, 1: 3–51.

Yakhot V, Orszag SA, Thangam S, Gatski TB, Speziale CG (1992). Development of turbulence models for shear flows by a double expansion technique. *Physics of Fluids A*: *Fluid Dynamics*, 4: 1510–1520.

Yakhot V, Smith LM (1992). The renormalization group, the ε–expansion and derivation of turbulence models. *Journal of Scientific Computing*, 7: 35–61.

Yang C (2012). Research of particles and droplets transmission characteristics and ventilation control strategy in laminar airflow ward. PhD Thesis, Tsinghua University, China. (in Chinese)

Yang B, Melikov A, Sekhar C (2009a). Performance evaluation of ceiling mounted personalized ventilation system. *ASHRAE Transactions*, 115 (2): 395–406.

Yang C, Yang X, Xu T, Sun L, Gong W (2009b). Optimization of bathroom ventilation design for an ISO Class 5 clean ward. *Building Simulation*, 2: 133–142.

Zhang T, Yin S, Wang S (2011). Quantify impacted scope of human expired air under different head postures and varying exhalation rates. *Building and Environment*, 46: 1928–1936.

Zhao B, Wu J (2005). Numerical investigation of particle diffusion in a clean room. *Indoor and Built Environment*, 14: 469–479.

Zoon WAC, Loomans MGLC, Hensen JLM (2011). Testing the effectiveness of operating room ventilation with regard to removal of airborne bacteria. *Building and Environment*, 46: 2570–2577.